

RESEARCH ARTICLE

Live applications of norbormide-based fluorescent probes in *Drosophila melanogaster*

Alessia Forgiarini¹, Zifei Wang², Claudio D'Amore¹, Morgan Jay-Smith², Freda Fan Li², Brian Hopkins³, Margaret Anne Brimble², Andrea Pagetta¹, Sara Bersani¹, Sara De Martin¹, Barbara Napoli⁴, Sergio Bova¹, David Rennison^{2*}, Genny Orso^{1*}

1 Department of Pharmaceutical and Pharmacological Sciences, University of Padova, Padova, Italy, **2** University of Auckland, School of Chemical Sciences, Auckland, New Zealand, **3** Landcare Research, Lincoln, New Zealand, **4** Scientific Institute IRCCS Eugenio Medea, Bosisio Parini, Lecco, Italy

* genny.orso@unipd.it (GO); d.rennison@auckland.ac.nz (DR)



Abstract

In this study we investigated the performance of two norbormide (NRB)-derived fluorescent probes, NRB^{MC009} (green) and NRB^{ZLW0047} (red), on dissected, living larvae of *Drosophila*, to verify their potential application in live cell imaging confocal microscopy. To this end, larval tissues were exposed to NRB probes alone or in combination with other commercial dyes or GFP-tagged protein markers. Both probes were rapidly internalized by most tissues (except the central nervous system) allowing each organ in the microscope field to be readily distinguished at low magnification. At the cellular level, the probes showed a very similar distribution (except for fat bodies), defined by loss of signal in the nucleus and plasma membrane, and a preferential localization to endoplasmic reticulum (ER) and mitochondria. They also recognized ER and mitochondrial phenotypes in the skeletal muscles of fruit fly models that had loss of function mutations in the atlastin and mitofusin genes, suggesting NRB^{MC009} and NRB^{ZLW0047} as potentially useful screening tools for characterizing ER and mitochondria morphological alterations. Feeding of larvae and adult *Drosophilae* with the NRB-derived dyes led to staining of the gut and its epithelial cells, revealing a potential role in food intake assays. In addition, when flies were exposed to either dye over their entire life cycle no apparent functional or morphological abnormalities were detected. Rapid internalization, a bright signal, a compatibility with other available fluorescent probes and GFP-tagged protein markers, and a lack of toxicity make NRB^{ZLW0047} and, particularly, NRB^{MC009} highly performing fluorescent probes for live cell microscopy studies and food intake assays in *Drosophila*.

OPEN ACCESS

Citation: Forgiarini A, Wang Z, D'Amore C, Jay-Smith M, Li FF, Hopkins B, et al. (2019) Live applications of norbormide-based fluorescent probes in *Drosophila melanogaster*. PLoS ONE 14(4): e0211169. <https://doi.org/10.1371/journal.pone.0211169>

Editor: Christian Wegener, Biocenter, Universität Würzburg, GERMANY

Received: January 7, 2019

Accepted: March 26, 2019

Published: April 8, 2019

Copyright: © 2019 Forgiarini et al. This is an open access article distributed under the terms of the [Creative Commons Attribution License](https://creativecommons.org/licenses/by/4.0/), which permits unrestricted use, distribution, and reproduction in any medium, provided the original author and source are credited.

Data Availability Statement: All relevant data are within the manuscript and its Supporting Information files.

Funding: This project was supported by the New Zealand Ministry of Business, Innovation and Employment's Endeavour Fund C09X1710 (BH, SBo, MB, GO, DR): <https://www.mbie.govt.nz/> and by the University of Padova, project n. 148125/14 (SBo) and SID18-01 (GO): <https://www.unipd.it/en/>. The funders had no role in study design, data

Introduction

Norbormide [5-(α -hydroxy- α -2-pyridylbenzyl)-7-(α -2-pyridylbenzylidene)-5-norbornene-2,3-dicarboximide] (NRB) is a selective rat toxicant that exhibits little or no non-target effects [1], and was developed and commercialized as an ecologic pesticide in the 1980s. Evidence suggests that the rat-selective action of NRB is mediated by a generalized vasoconstrictor effect

collection and analysis, decision to publish, or preparation of the manuscript.

Competing interests: The authors have declared that no competing interests exist.

that has only been observed in the rat peripheral blood vessels, both *in vivo* and *in vitro*. In contrast, NRB displays a vasorelaxant action in arteries from non-rat species, as well as in rat aorta and extravascular smooth muscle, that has been proposed to be the result of a reduction of Ca^{2+} entry through L-type Ca^{2+} channels [2,3]. The molecular mechanism underlying NRB-induced vasoconstriction is not known, however, it has been proposed that the compound acts on rat vascular myocytes where it activates the PLC-IP3-PKC pathway [2], a signaling cascade stimulated by most receptor-coupled vasoconstrictor agents [4]. In an attempt to identify the cellular targets of NRB, we previously developed fluorescent derivatives of the parent compound by linking it to either nitrobenzoxadiazole (NBD) or boron-dipyromethene (BODIPY FL) fluorophores, and found that both were able to clearly label intracellular structures such as endoplasmic reticulum (ER), Golgi apparatus, mitochondria, and lipid droplets (LDs) in various cell lines, in the absence of cytotoxic effects. Based on these results, we proposed NRB as a scaffold for the development of new, high performing, non-toxic fluorescent probes for live cell imaging [5,6].

Drosophila melanogaster is an animal model widely used to investigate the biochemical pathways and the cellular/subcellular morphological alterations that characterize human diseases [7–12]. Confocal fluorescent microscopy live cell imaging is a particularly informative methodology in this model, especially when fluorescent probes are used in combination with genetic tools (e.g. mutant flies, RNA interference, fluorescently marked proteins, Gal4/UAS activation system) [13,14], allowing the visualization of dynamic biological processes in living systems without the artifacts often generated by sample fixation procedures [15].

In this study, we investigated the performance of two NRB-derived fluorescent probes, the previously developed NRB^{MC009} (green fluorescence) and the newly developed NRB^{ZLW0047} (red fluorescence), on dissected, living third instar larvae of *Drosophila melanogaster*, to assess their potential application in live cell imaging confocal microscopy. In particular, we were able to characterize the distribution of NRB^{MC009} and NRB^{ZLW0047} to cellular structures and organelles in tissues of wild-type *Drosophila* larvae, as well as in tissues of mutant lines exhibiting morphological alterations of endoplasmic reticulum and mitochondria. Finally, we explored if these probes could be useful for studying fruit fly feeding and gut morphology.

Material and methods

NRB^{MC009} and NRB^{ZLW0047} synthesis

NRB^{MC009}, a BODIPY FL derivative of norbormide, was synthesized as previously reported [6]. Stock solutions 1 mM in DMSO were prepared and maintained at -20°C and diluted to the desired concentration before each experiment.

NRB^{ZLW0047}, a BODIPY TMR derivative of norbormide, was prepared as follows: BODIPY TMR (4,4-difluoro-5-(4-methoxyphenyl)-1,3-dimethyl-4-bora-3a,4a-diaza-s-indacene-2-propionic acid) [16], along with its corresponding N-hydroxysuccinimide ester, BODIPY TMR NHS ester [16], and N-2'-aminoethyl-endo-5-(α -hydroxy- α -2-pyridylbenzyl)-7-(α -2-pyridylbenzylidene)-5-norbornene-2,3-dicarboximide [17] were prepared using literature methods. A solution of N-2'-aminoethyl-endo-5-(α -hydroxy- α -2-pyridylbenzyl)-7-(α -2-pyridylbenzylidene)-5-norbornene-2,3-dicarboximide (111 mg, 0.20 mmol), BODIPY TMR NHS ester (110 mg, 0.20 mmol) and *N,N*-diisopropylethylamine (35 μ l, 0.20 mmol) in dichloromethane (7 ml) was stirred at room temperature for 16 h. The mixture was then diluted with dichloromethane (20 ml), washed with water (10 ml), the separated aqueous phase further extracted with dichloromethane (2 \times 10 ml), the combined organic layers washed with brine (3 \times 20 ml), dried over anhydrous magnesium sulfate, filtered and the solvent removed *in vacuo*. Purification by flash chromatography (petroleum ether/ethyl acetate, 1:3) afforded NRB^{ZLW0047} as a

mixture of endo stereoisomers (purple solid; 70 mg, 37%). ^1H NMR (400 MHz, CDCl_3) δ 8.64–8.38 (2H, m, αPyr), 7.88–7.82 (2H, m, ArH), 7.59–6.77 (20H, m, ArH), 6.53–6.47 (1H, m, C = CH), 6.29 (0.2H, br s, OH), 6.28 (0.1H, br s, OH), 6.21–6.20 (0.2H, m, W/H-6), 6.15–6.14 (0.1H, m, U/H-6), 5.54–5.53 (0.4H, m, Y/H-6), 5.52–5.51 (0.3H, m, V/H-6), 5.22 (0.4H, br s, OH), 5.15 (0.3H, br s, OH), 4.49–4.46 (0.2H, m, W/H-1), 4.46–4.43 (0.4H, m, Y/H-1), 4.31–4.29 (0.3H, m, V/H-1), 4.03–4.01 (0.1H, m, U/H-1), 3.85–3.84 (3H, m, OMe), 3.84–3.24 (7H, m, H-2, H-3, H-4 and NCH_2CH_2), 2.75–2.72 (2H, m, COCH_2CH_2 or COCH_2CH_2), 2.47 (3H, m, Me), 2.26–2.22 (2H, m, COCH_2CH_2 or COCH_2CH_2), 2.20–2.18 (3H, m, Me).

Stock solutions 1 mM in DMSO were prepared and maintained at -20°C and diluted to the desired concentration before each experiment.

Fluorescence spectra

Excitation and emission spectra of $\text{NRB}^{\text{MC009}}$ and $\text{NRB}^{\text{ZLW0047}}$ were obtained by diluting the stock solution in Milli-Q water to reach the final concentration of 2 μM . To verify that the medium used for *Drosophila* live imaging (HL3) had no effect on the emission spectra, a comparison was made between probes diluted in water and probes diluted in HL3—no variation in fluorescence was observed.

Analysis of excitation/emission peaks were evaluated using a Jasco FP6500 spectrofluorometer (temperature 25°C ; b = 1 cm; λ ex/em: 470/540 for $\text{NRB}^{\text{MC009}}$ and 545/580 for $\text{NRB}^{\text{ZLW0047}}$; sli: 5/10 nm; data pitch 0.2 nm; scanning speed 200nm/min).

Fly stocks

Drosophila melanogaster strains used: $w^{[1118]}$ (BL-5905), Tubulin-Gal4 (BL-5138), UAS-Mito-GFP (BL-8443), UAS-mCD8-GFP (BL-5130), were obtained from Bloomington Drosophila Stock Center, and UAS-ATL2^{RNAi} [18] and UAS-Marf^{RNAi} (ID 40478), were resourced from Vienna Drosophila Resource Center. UAS-Lamp-GFP was provided by Helmut Krämer (University of Texas Southwestern Medical Center, Dallas), and UAS-HneuGFP was generated by cloning HNEU-GFP [19] in pUASTattB, and transgenic lines generated by BestGene Inc, (Chino Hills, CA, USA). $w^{[1118]}$ flies were maintained on standard food at 25°C , and Gal4/UAS crossings were performed at 28°C . Starvation was induced by leaving third instar larvae for 6 hours in 20% sucrose dissolved in PBS.

Larval dissection

Fly larvae having reached the third instar stage were pinned between the posterior spiracles and above the mouth hooks in a Sylgard dissection dish, and cut along the dorsal midline. Hemolymph-like (HL3) saline (70 mM NaCl, 5 mM KCl, 1.5 mM CaCl_2 , 20 mM MgCl_2 , 10 mM NaHCO_3 , 5 mM trehalose, 115 mM sucrose, 5 mM sodium HEPES, pH 7.2, all supplied by Sigma-Aldrich) was added and the lateral flaps were fastened with four needles to stretch the body wall. All larval organs were left on the muscle fillet for whole larval acquisition, whereas for single tissue acquisition the unnecessary organs were removed.

Live tissue imaging

To characterize $\text{NRB}^{\text{MC009}}$ and $\text{NRB}^{\text{ZLW0047}}$ localization, each were diluted in HL3 medium at concentrations of 500 nM and 1 μM , respectively, and were added to the dissected larva and images acquired after 15 min. For $\text{NRB}^{\text{MC009}}$ colocalization studies, ER-Tracker Red 2 μM (BODIPY TR Glibenclamide), MitoTracker Orange CMTMRos 1 μM , LysoTracker Deep Red 2 μM , HCS LipidTOX Deep Red Neutral Lipid Stain 1:100, or CellMask Orange 1 μM (all by

Thermo Fisher, respectively #E34250, #M7510, #L12492, #H34477, and #10045) were added, together with NRB^{MC009} at 500 nM. To verify NRB^{ZLW0047} colocalization with other organelles, it was added on dissected larvae expressing GFP-tagged proteins (Hneu-GFP, Mito-GFP, Lamp-GFP, and mCD8-GFP), or together with BODIPY 493/503 dye 10 µg/ml (#D3922, Thermo Fisher). In order to test tissue autofluorescence, dissected larvae were imaged in HL3 medium without fluorescent probes with identical laser settings of labeled tissues (S1 Fig). Whole larvae images and magnifications were acquired using a Zeiss LSM800 Axio Observer Z1 inverted microscope equipped with a Zeiss Plan-Apochromat 5x/0.15 ph1 or 40x/0.95 objectives, all other images were acquired with a Nikon D-Eclipse C1 confocal microscope equipped with a Nikon Plan Apo 60x/1.40 or a Nikon Plan Apo 40x/1.0 oil immersion objectives.

Three-choice preference assay

To test larval food preference, a Petri dish was divided in three quadrants filled with a warm liquefied standard food solution. In two quadrants, the food contained either NRB^{MC009} or NRB^{ZLW0047} (both 20 µM), in the third the food was left probe-free. At the beginning of the experiment, a group of 10 larvae was placed in the middle of the assay plate and after 5 min the number of larvae on each quadrant was counted [20]. The experiment was repeated five times.

Food intake test

The food intake test was conducted in third instar larvae starved for 1 hour in 20% sucrose dissolved in PBS. The starved larvae were then divided into three groups, separately fed with brilliant blue R dye 0.08%, NRB^{MC009}, or NRB^{ZLW0047} (both at a concentration of 20 µM) dissolved in liquid food (sucrose 20% and 20% dry yeast in PBS) for 30 min [21], frozen at -80°C and imaged using a Leica MZ 16 FA microscope. To estimate food intake, the area of dye-labeled gut, visible through the cuticle, was quantified relative to larval total body area. 10 larvae for each experiment were used and the experiment was repeated three times. Image analysis was performed with ImageJ 1.52h software.

Analysis of gut fluorescence in *Drosophila* chronically fed with NRB^{MC009} and NRB^{ZLW0047}

Third instar larvae, grown in NRB^{MC009}- and NRB^{ZLW0047}- enriched food as described in the chronic toxicity assay, were collected and food debris was removed by washing in PBS for 5 minutes and 70% ethanol for 1 minute and then dissected, being careful to not cut the digestive tract. Images were acquired using a Zeiss Axio Observer Z1 inverted microscope equipped with a Zeiss Plan-Apochromat 5x/0.15 ph1 or 40x/0.95 objectives.

Chronic toxicity assay

The toxicity of NRB-derived probes was investigated by exposing the flies to NRB^{MC009} or NRB^{ZLW0047} 20 µM over the entire life-cycle (mating, eggs maturation, pupal development, eclosion). Male and female w^[1118] flies were placed in a tube with standard food containing vehicle, NRB^{MC009}, or NRB^{ZLW0047} 20 µM, and grown at 25°C. After 5–6 days, parent flies were removed and analyzed to verify probe intake. Eggs were left to develop in food containing one of each of the NRB fluorescent probes until the eclosion. Two parameters were considered in the evaluation of toxicity: 1) eclosion rate (percent of emerged flies versus the total number of pupae, including the dead ones); 2) morphological alterations of eclosed adults. Morphological

alterations of male and female adult body, eyes, wings, and legs were evaluated and imaged using a Leica MZ 16 FA microscope.

Statistical analysis

Analysis of colocalization was performed using Pearson's correlation coefficient calculated with Coloc2 plugin of Fiji [22]. All values are expressed as means \pm standard error of the mean (SEM) of n observations ($n \geq 10$). The significance of the probes fluorescence intensity versus background subtracted fluorescence intensity was calculated using unpaired t test. The significance of the three-choice assays, food intake tests and eclosion rate was calculated using One-way ANOVA test followed by Tukey's Multiple Comparison Test, using GraphPad Prism 6.01.

Results and discussion

Synthesis and excitation/emission spectra of fluorescent probes NRB^{MC009} and NRB^{ZLW0047}

The structures and synthetic routes to generate NRB^{MC009} and NRB^{ZLW0047} are summarized in Fig 1A and 1B, respectively. The excitation and emission spectra of the dyes in water, and in the physiological buffer (HL3) solution, which was used to perform live imaging experiments in *Drosophila* tissues, are presented in Fig 1C and 1D, respectively, and summarized in Fig 1E. The excitation spectra analysis showed that the probes can be excited using the common laser lines 561 nm (NRB^{ZLW0047}) and 488 nm (NRB^{MC009}), respectively.

Tissue distribution of NRB^{MC009} and NRB^{ZLW0047} in *Drosophila* larvae

To characterize NRB^{MC009} and NRB^{ZLW0047} fluorescence distribution in *Drosophila* tissues, we dissected a wild type larva and exposed the whole body to the fluorescent probes. Figs 2A and 3A are confocal images of dissected third instar larvae in which all tissues were left intact and labeled with 500 nM NRB^{MC009} or 1 μ M NRB^{ZLW0047}, respectively. As shown in the pictures, both dyes localized to most of the tissues, with an apparent brighter signal detected in imaginal discs, tracheal system, salivary glands, and fat body (Fig 2B, 2D, 2H and 2J, respectively, and Fig 3B, 3H and 3J, respectively), and a less intense signal being detected in muscular tissues, oenocytes, the entire digestive tract, the ring gland, and epidermal cells (Fig 2C, 2E, 2F, 2G, 2I and 2K, respectively, and Fig 3C, 3E, 3F, 3G, 3I and 3K, respectively). NRB^{MC009} and NRB^{ZLW0047} were unable to label the central nervous system i.e. ganglion, brain lobes, and nerves (dotted boxes on Figs 2A and 3A). In order to exclude possible autofluorescence disturbance, all tissues were captured under the same laser conditions without probe labeling; as shown in S2A–S2J Fig, tissues autofluorescence is almost null and does not interfere with the emission intensity of NRB^{MC009} and NRB^{ZLW0047} (S2K and S2L Fig).

The labeling properties of the two probes were compared by co-loading larval tissues with both dyes, and merging the corresponding images for colocalization analysis. The results, reported in Fig 4A–4D, indicate that both dyes were able to penetrate the cells of the tissues, and effectively label the intracellular structures. Cell internalization of the dyes was very rapid, allowing a clear visualization of the intracellular structures in less than 2 minutes (S1 and S2 Videos and S3 Fig). Pearson's coefficient results (Fig 4E and 4F) confirmed that NRB^{MC009} and NRB^{ZLW0047} recognized the same intracellular structures in most of the tissues investigated. However, a clear difference in subcellular expression between NRB^{MC009} and NRB^{ZLW0047} was observed in the fat bodies, in which lipid droplets (LDs) were selectively stained by NRB^{MC009}

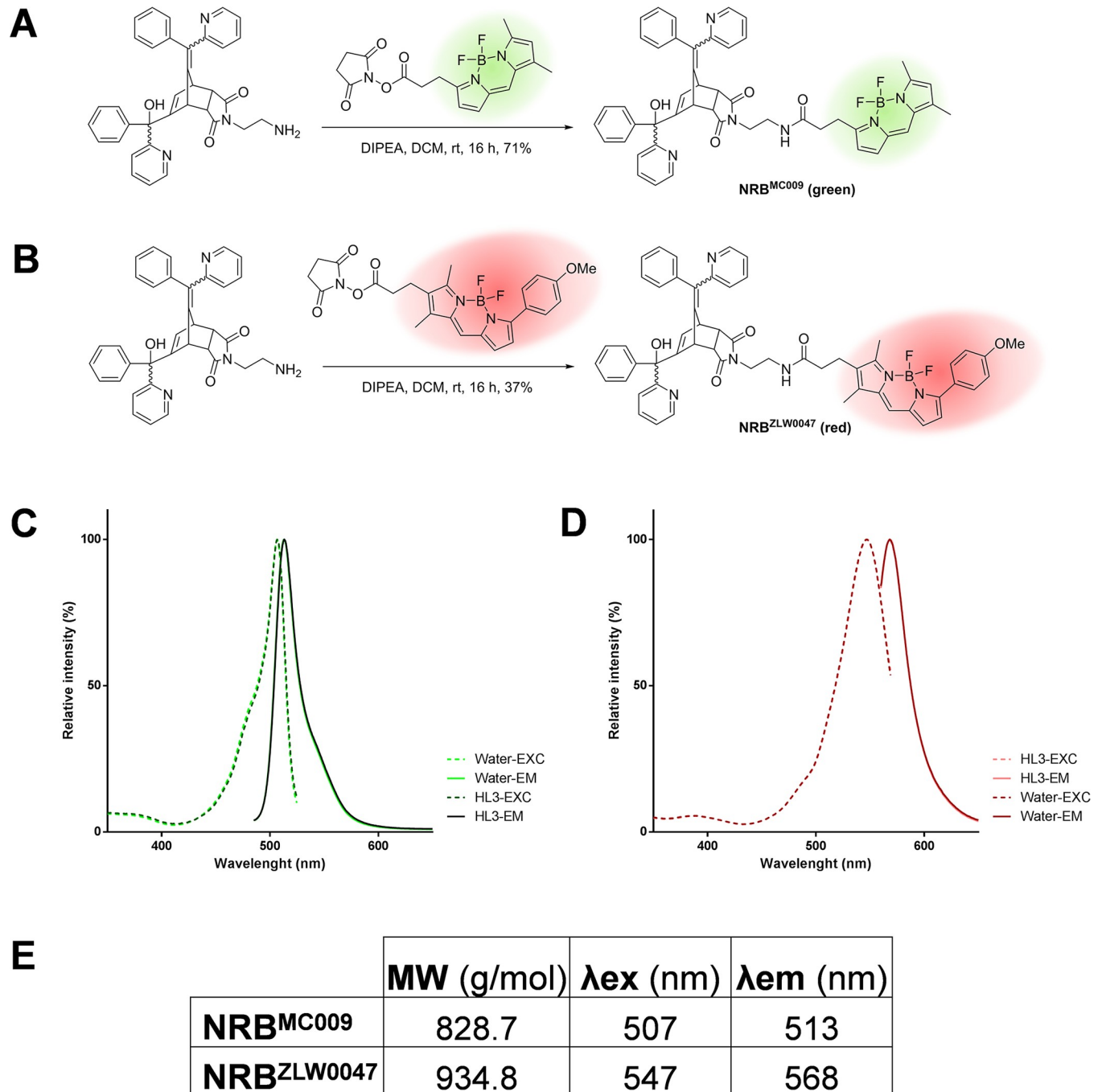


Fig 1. NRB^{MC009} and NRB^{ZLW0047} synthesis and fluorescent spectra. Scheme of the synthesis of NRB^{MC009} (A) and NRB^{ZLW0047} (B). Excitation and emission spectra of NRB^{MC009} (C) and NRB^{ZLW0047} (D) diluted in water (light color) or in HL3 medium (dark color). Summary table of physical properties of NRB^{MC009} and NRB^{ZLW0047} (E), MW: molecular weight; λ_{exc} : excitation wavelength; λ_{em} : emission wavelength.

<https://doi.org/10.1371/journal.pone.0211169.g001>

(Fig 4B). This behavior may reflect a different binding capacity of the two probes to the constituents of LDs, i.e. neutral lipids, mainly triacylglycerols and sterol esters, and phospholipids [23,24].

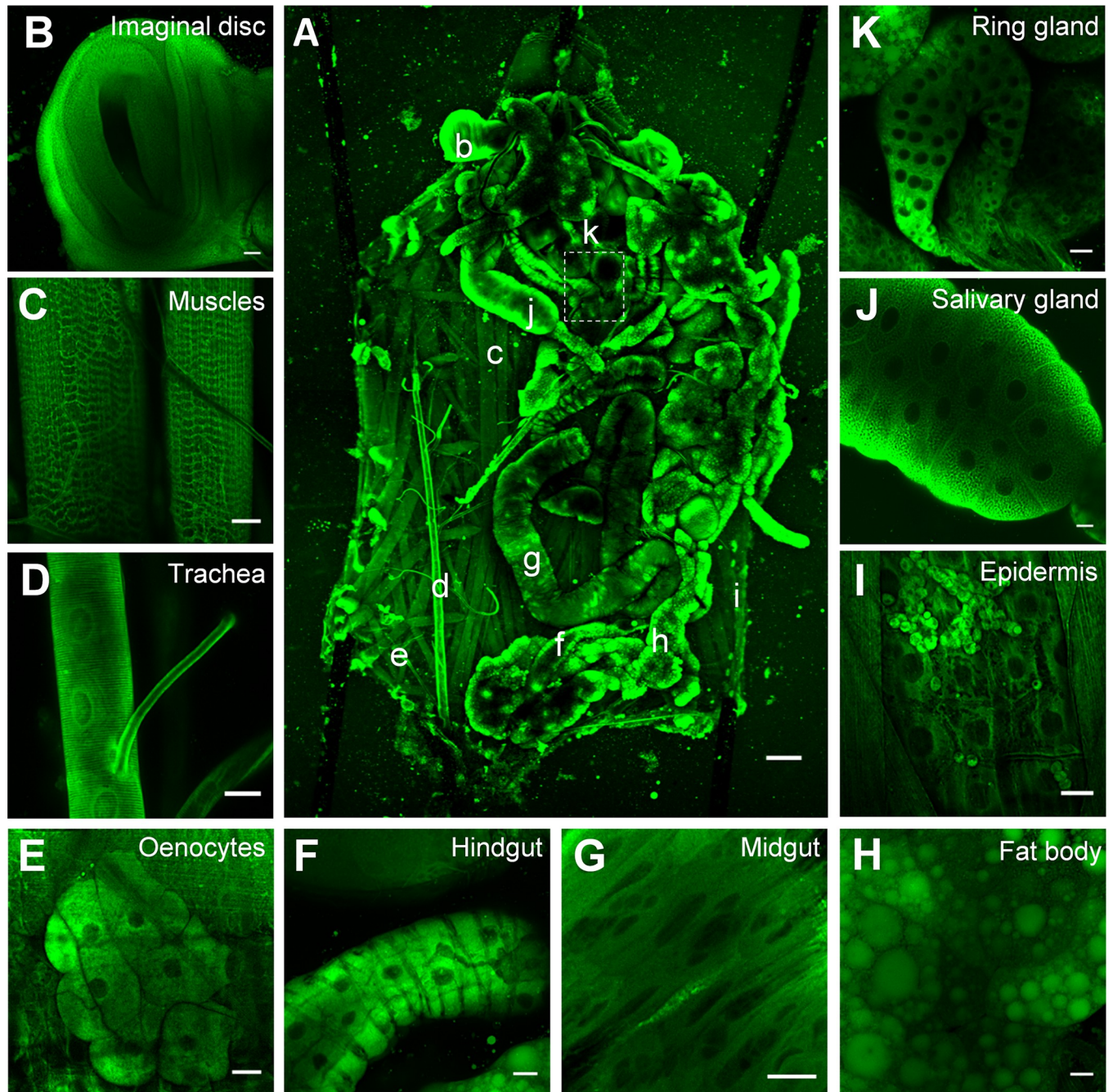


Fig 2. NRB^{MC009} distribution in *Drosophila* larval tissues. Confocal live imaging of (A) whole dissected w^{1118} third instar larva labeled with NRB^{MC009} 500 nM. Small letters reveal corresponding magnified tissues, dotted box shows unlabeled central nervous system (CNS). Magnification 5x; scale bar 200 μ m. Detailed images of (B) leg imaginal disc, (C) muscles, (D) trachea, (E) oenocytes, (F) hindgut, (G) midgut, (H) fat body, (I) epidermis and hematocytes, (J) salivary gland, and (K) ring gland; magnification 40x; scale bars 20 μ m.

<https://doi.org/10.1371/journal.pone.0211169.g002>

Cellular distribution of NRB^{MC009} and $NRB^{ZLW0047}$

We next characterized the cellular structures labeled by NRB^{MC009} and $NRB^{ZLW0047}$. In all the tissues investigated, we found that both probes allowed the visualization of intracytoplasmic organelles but did not penetrate the nuclei (S4 Fig). Furthermore, neither probe was able to

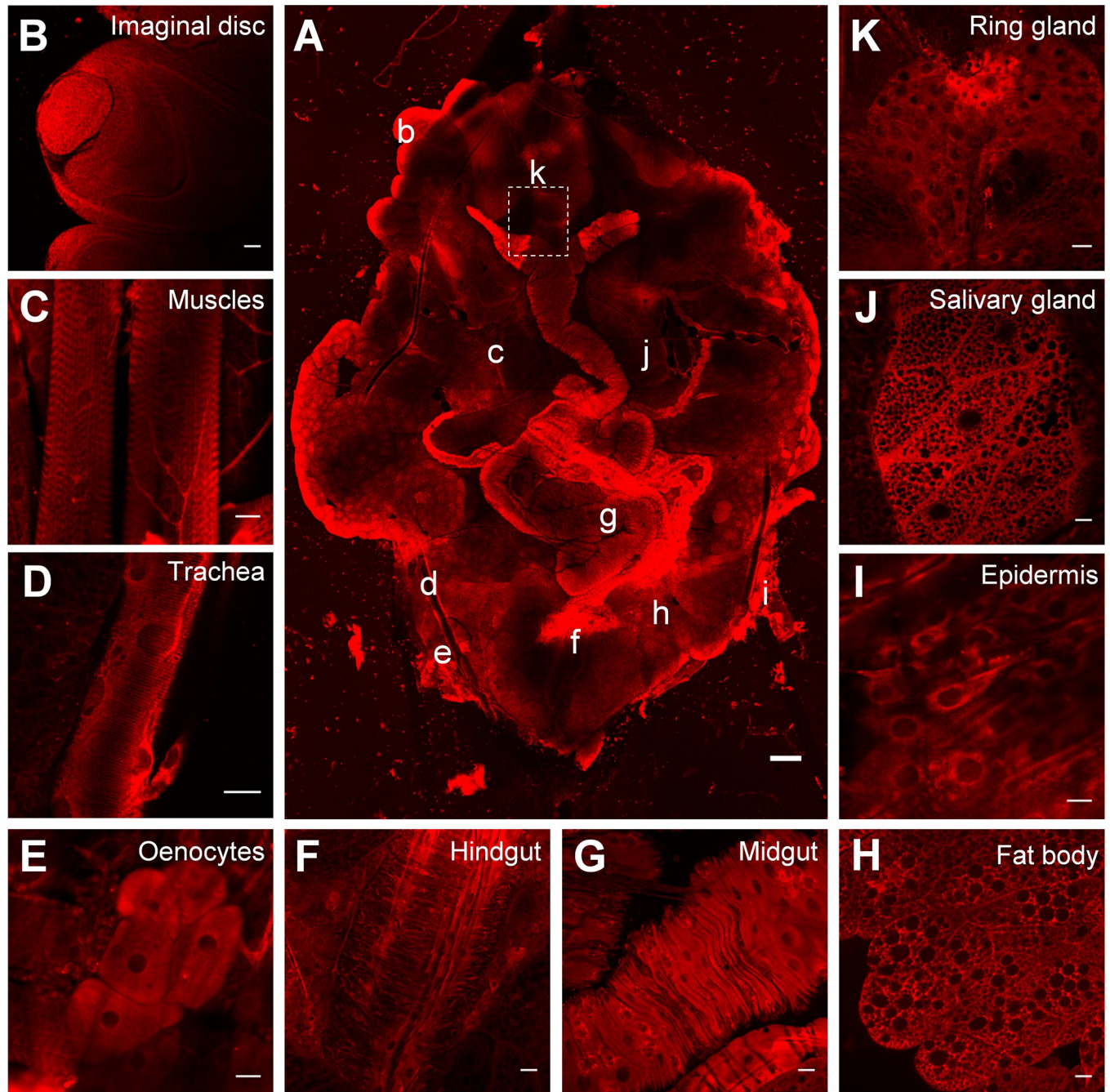


Fig 3. NRB^{ZLW0047} distribution in *Drosophila* larval tissues. Confocal live imaging of (A) whole dissected *w^[1118]* third instar larva labeled with NRB^{ZLW0047} 1 μ M. Small letters reveal corresponding magnified tissues, dotted box shows unlabeled CNS. Magnification 5x; scale bar 200 μ m. Detailed images of (B) leg imaginal disc, (C) muscles, (D) trachea, (E) oenocytes, (F) hindgut, (G) midgut, (H) fat body, (I) epidermis, (J) salivary gland, and (K) ring gland; magnification 40x; scale bars 20 μ m.

<https://doi.org/10.1371/journal.pone.0211169.g003>

label plasma membrane as shown by experiments using CellMask Orange dye (S4A–S4E Fig) and in larval tissues expressing mCD8-GFP (S4F–S4L Fig).

The intracellular distribution of NRB^{MC009} and NRB^{ZLW0047} was analyzed in more detail in *Drosophila* larval musculature in which we investigated the binding of these NRB fluorescent

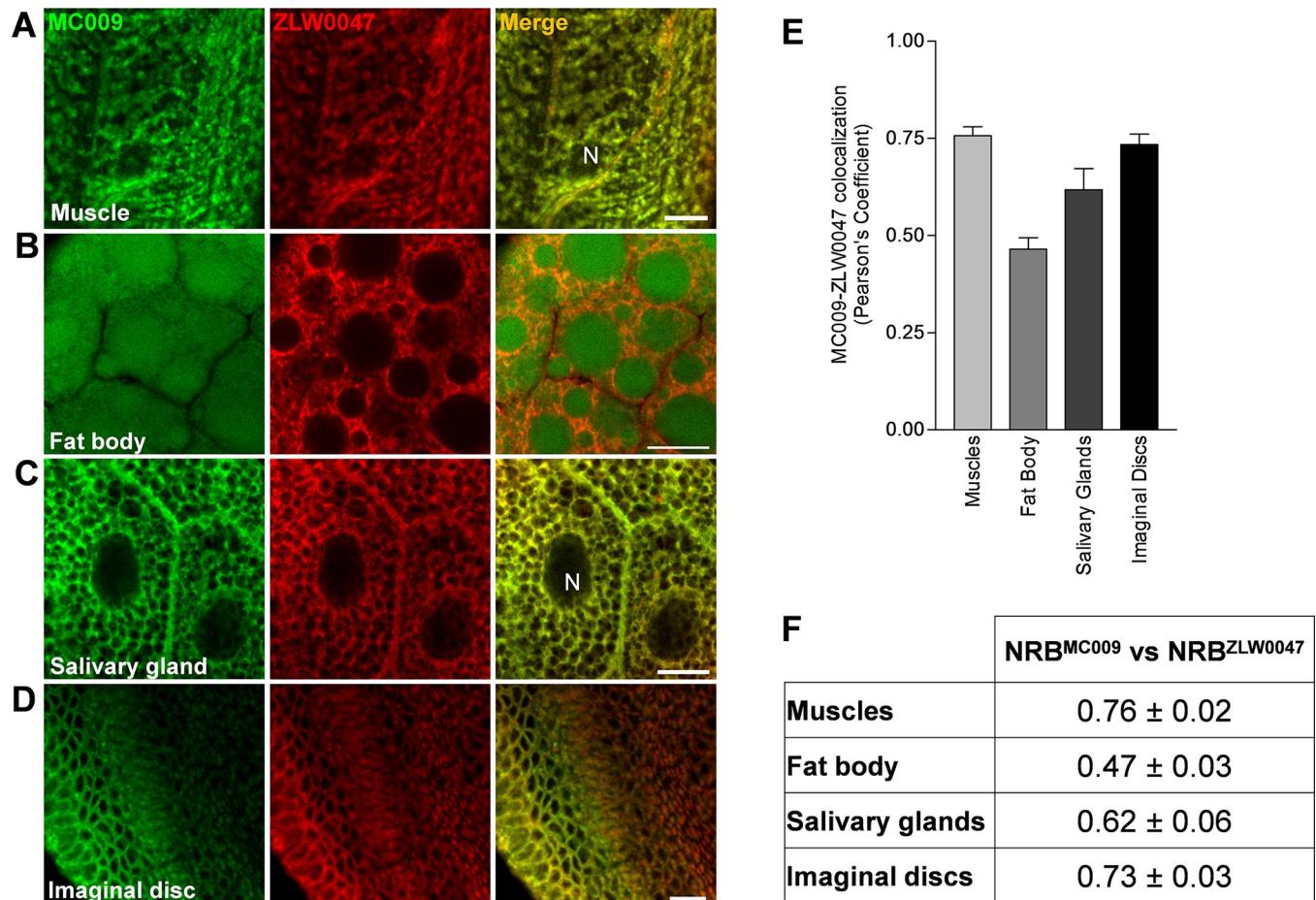


Fig 4. NRB^{MC009} and NRB^{ZLW0047} colocalization. Confocal live imaging of dissected *w¹¹¹⁸¹* third instar larval (A) muscle, (B) fat body, (C) salivary gland, and (D) imaginal disc labeled with NRB^{MC009} 500 nM (green) together with NRB^{ZLW0047} 1 μM (red). Magnification 60x; scale bars 10 μm. Graph (E) and summary table (F) of Pearson's correlation coefficients between NRB^{MC009} and NRB^{ZLW0047} in the evaluated tissues. Data are expressed as mean ± SEM, n ≥ 10.

<https://doi.org/10.1371/journal.pone.0211169.g004>

derivatives to ER, mitochondria, lysosomes and LDs. The larval body wall muscles provide a relatively simple system to study development of muscles, cytoskeleton dynamics, intracellular trafficking and neuromuscular junction dysfunction. In fact, besides the well-known actin and myosin filaments and their associated proteins, muscles also contain a cytoskeleton, intracellular organelles of the endo-lysosomal pathway, and well-defined endoplasmic reticulum and mitochondrial networks [25]. We focused on these particular structures because we recently showed that they contained a significant density of binding sites for NRB^{MC009} [6]. To study the intracellular localization of NRB^{MC009} we co-loaded it into larval muscle with organelle-specific red fluorescent dyes. To confirm NRB^{ZLW0047} localization we profiled it in larval muscles labelled with organelle-selective green fluorescent proteins.

The results, showed good co-localization of NRB^{MC009} with ER tracker Red (ER probe, Pearson's coefficient 0.65 ± 0.03, Fig 5A), Mitotracker Orange (mitochondrial probe, Pearson's coefficient 0.54 ± 0.05, Fig 5B) and LipidTOX (lipid droplets probe, Pearson's coefficient 0.42 ± 0.02, Fig 5C); however, NRB^{MC009} did not colocalize with LysoTracker Deep Red (a lysosome probe, Pearson's coefficient 0.04 ± 0.04, Fig 5D). The localization of NRB^{ZLW0047} was confirmed using green fluorescent-tagged proteins that specifically targeted the ER (UAS-H-neu-GFP), mitochondria (UAS-Mito-GFP) and lysosomes (UAS-Lamp-GFP), and BODIPY

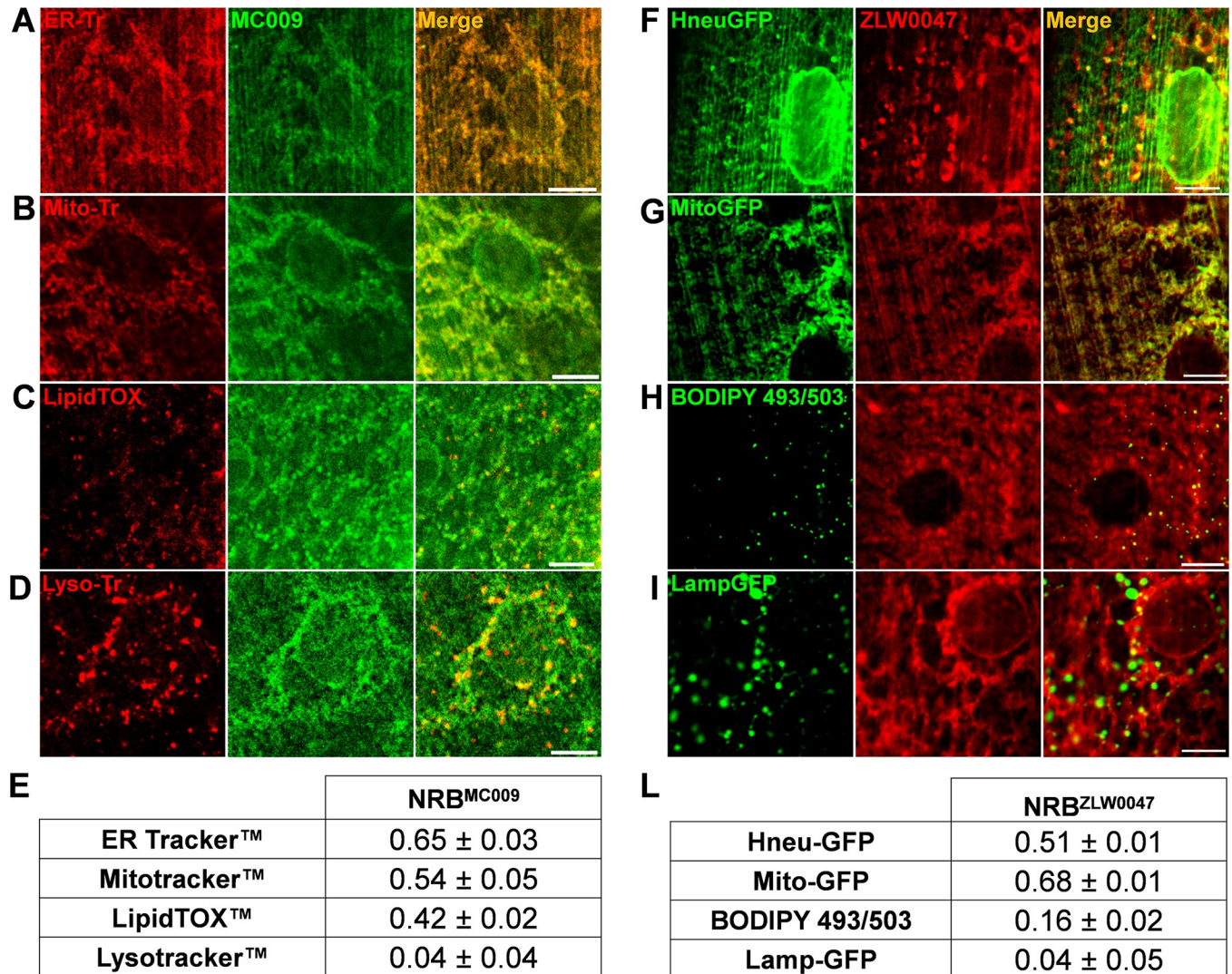


Fig 5. NRB^{MC009} and NRB^{ZLW0047} intracellular distribution in larval muscles. Confocal live imaging of w^[1118] third instar larval muscles 6–7 from segment A3 labeled and ER-tracker 2 μM (ER marker, A), Mitotracker 1 μM (mitochondria marker, B), LipidTOX 1:100 (LDs marker, C), and Lyso-tracker 2 μM (lysosomes marker, D), all in red, together with NRB^{MC009} 500 nM (green). Magnification 60x; scale bars 10 μm. Summary table of Pearson's correlation coefficients between NRB^{MC009} and fluorescent organelle-marker probes used in larval muscles (E). Data are expressed as mean ± SEM, n ≥ 10. Confocal live imaging of third instar larval muscles 6–7 from segment A3 of UAS-Hneu-GFP/Tubulin-Gal4 (ER marker, F), UAS-Mito-GFP/Tubulin-Gal4 (mitochondrial marker, G), w^[1118] added with BODIPY 493/503 10 μg/ml (LDs marker, H), and UAS-Lamp-GFP/+;Tubulin-Gal4/+ (Lysosomes marker, I), all labeled with NRB^{ZLW0047} 1 μM (red). Magnification 60x; scale bars 10 μm. Summary table of Pearson's correlation coefficients between NRB^{MC009} and fluorescent organelle-markers in *Drosophila* larval muscles (L). Data are expressed as mean ± SEM, n ≥ 10.

<https://doi.org/10.1371/journal.pone.0211169.g005>

493/503 dye that targeted the LDs. The results, shown in Fig 5E–5H, demonstrated that the distribution of NRB^{ZLW0047} partially overlapped that of NRB^{MC009}; that both NRB^{MC009} and NRB^{ZLW0047} exhibited good labeling of ER and mitochondria (Pearson's coefficient 0.51 ± 0.01 and 0.68 ± 0.01, respectively, Fig 5F and 5G); that both were absent in lysosomes (Pearson's coefficient 0.04 ± 0.02, Fig 5I); and that they differed in their localization in LDs, where NRB^{MC009} fluorescence was present (Pearson's coefficient 0.42 ± 0.02, see also Fig 5C) but NRB^{ZLW0047} fluorescence was absent (Pearson's coefficient 0.16 ± 0.05, Fig 5H).

These data show that both compounds, but particularly NRB^{MC009}, can be used to visualize and distinguish most organs/tissues of the dissected living larvae, and allow good definition of

their intracellular structures. In addition, the co-localization studies revealed that both NRB^{MC009} and NRB^{ZLW0047} labelled subcellular organelles, that they preferentially targeted the ER and mitochondria, and that they were totally absent from the nuclei, plasma membranes and lysosomes, which is in agreement with data reported in mammalian cell studies [6]. Moreover, the efficiency of the probes was tested with two different approaches: 1) in combination with commercially available dyes for live imaging, and 2) together with green fluorescent proteins that label specific cellular structures. In both the experimental backgrounds the NRB based probes allowed the identification of endoplasmic reticulum and mitochondria structures, making both probes useful new markers in *Drosophila* studies. Based on the capability of these dyes to recognize the same intracellular structures in both mammalian and fruit fly cells, their potential use in more complex animal models is anticipated. Subsequently, our ongoing work is focused on the development of these probes as tools to allow live imaging studies to be conducted in mouse and rat tissues.

NRB^{MC009} and NRB^{ZLW0047} cellular distribution in pathologic mutation-related phenotypes

In consideration of the preferential distribution of NRB-derived fluorescent probes to ER and mitochondria we next verified if they could be developed into tools to highlight phenotypic modifications of the ER and mitochondrial networks in *Drosophila* muscles. A large number of human disease genes are conserved in *Drosophila* and its genome can be easily manipulated to recreate and study human pathologic phenotypes [26]; subsequently, *Drosophila* is widely used as a model to study muscle growth, degeneration and correlated diseases [27–30].

In this study NRB^{MC009} and NRB^{ZLW0047} were tested on two *Drosophila* pathologic models: Charcot–Marie–Tooth disease (CMTd) and hereditary spastic paraplegia (HSP) [31,32].

CMTd *Drosophila* phenotype was obtained by inducing a downregulation of *Marf*, the fruit fly orthologue of the human gene *Mitofusin2*, which encodes for a GTPase that, together with Opa1, fuses mitochondria; mutations of this gene are implicated in CMT disease [33]. The depletion of this protein in *Drosophila* is known to cause fragmented and clustered mitochondria in neuronal cell bodies and to disorganize the typical sarcomeric location of mitochondria in the larval muscles, clumping them mainly around the nuclei [34]. Fig 6B shows the fluorescent distribution of NRB^{MC009} and NRB^{ZLW0047} in muscles of larvae in which *Marf* had been ubiquitously downregulated (UAS-*Marf*^{RNAi}/Tubulin-Gal4). Since these fluorescent images are comparable with those previously reported with the mitochondrial marker UAS-Mito-GFP [34] in the same model, when considering the mitochondrial labeling properties of NRB^{MC009} and NRB^{ZLW0047} (this study), it can be argued that fluorescent derivatives of NRB are able to also stain altered mitochondria, and be able to highlight pathologic mitochondrial phenotypes.

HSP *Drosophila* phenotype was obtained by inducing a downregulation of atlastin. Atlastins are membrane-bound dynamin-like GTPases implicated in ER network morphogenesis, and mutations in *atlastin1* gene are involved in the onset of a common form of HSP (SPG3A). *Drosophila* holds a unique highly conserved *atlastin* orthologue, and its downregulation elicits a fragmented ER in neurons and an enrichment of ER punctae localized in the proximity of nuclei, and visualized using UAS-KDEL-GFP [18]. Labeling of larva fillets with NRB^{MC009} and NRB^{ZLW0047} revealed a different pattern between muscles of wild type (Fig 6A) and atlastin-downregulated (UAS-*Atl*^{RNAi}/Tubulin-Gal4) larvae (Fig 6C), in which a brighter perinuclear signal, compatible with the previously described HSP phenotype, is observed.

Taken together, these results indicate that NRB^{MC009} and NRB^{ZLW0047} could be useful tools for *Drosophila* live imaging to highlight phenotypes attributable to mutations in, and/or

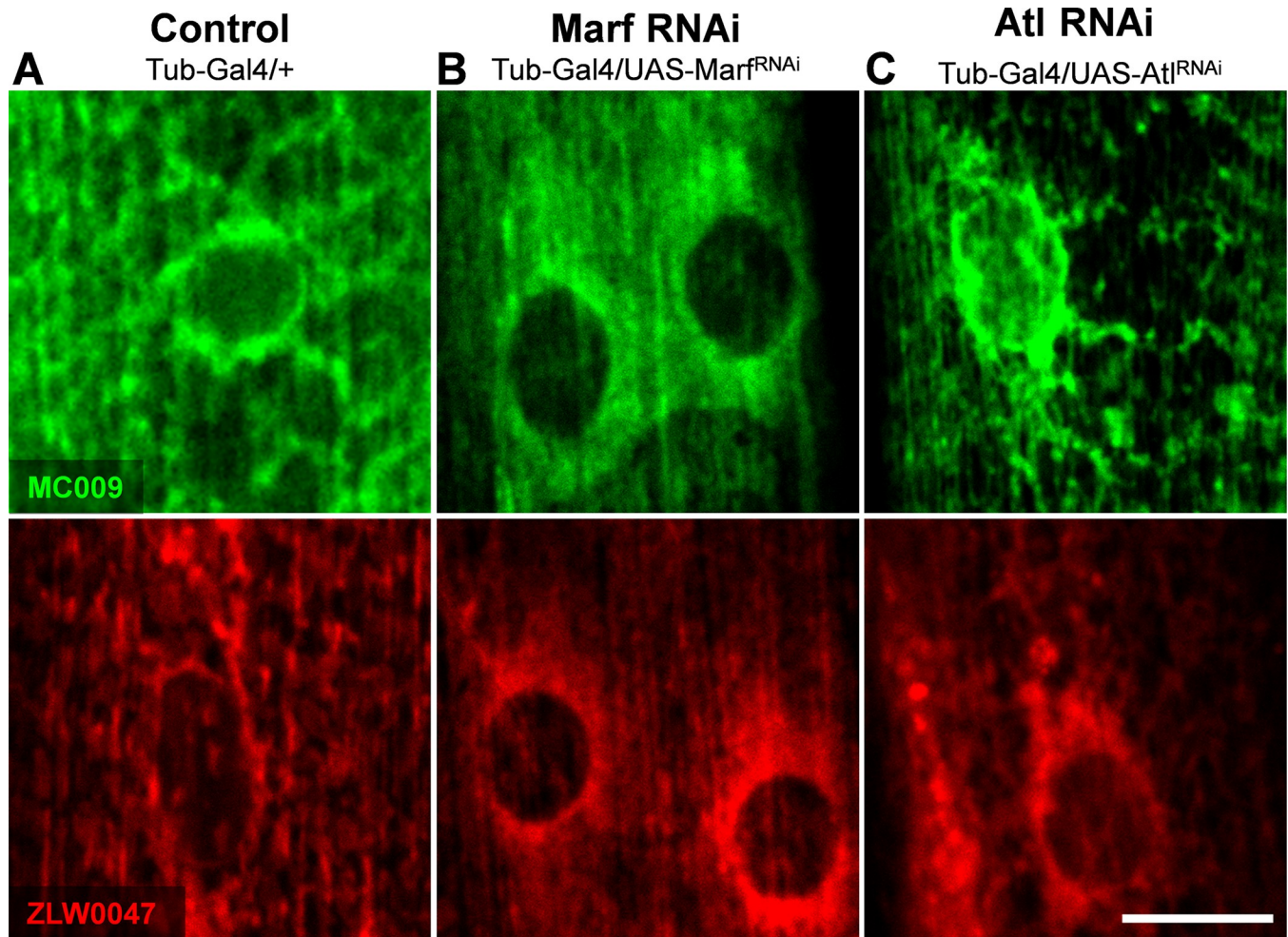


Fig 6. NRB^{MC009} and NRB^{ZLW0047} highlight pathologic mutation related phenotypes. Confocal live imaging of *Drosophila* muscles 6–7 from segment A3 of (A) control (Tubulin-Gal4/+), (B) Marf downregulation (UAS-Marf^{RNAi}/Tubulin-Gal4), and (C) atlastin downregulation (UAS-Atlastin^{RNAi}/Tubulin-Gal4) labeled with NRB^{MC009} 500 nM (green) or NRB^{ZLW0047} 1 μ M (red). Magnification 60x; scale bars 10 μ m.

<https://doi.org/10.1371/journal.pone.0211169.g006>

downregulation of genes implicated in mitochondria and/or endoplasmic reticulum network modifications. In addition, the short time it takes for these probes to permeate and label tissue and their general ease of use, means that both could be used as tools in compound screening studies to identify candidates that would help alleviate any network malfunction due to genetic modification.

NRB^{MC009} and NRB^{ZLW0047} in food intake tests

Next we explored the possibility of using NRB^{MC009} and NRB^{ZLW0047} as tools to evaluate food intake and to investigate potential gut morphological modifications in *Drosophila in vivo*. By adopting a three-choice test (behavioral choice test) we verified that NRB^{MC009} and NRB^{ZLW0047}, when added to the food, were accepted by the flies. As summarized in Fig 7A, there were no substantial differences in food preference between the standard diet and NRB^{MC009}- and NRB^{ZLW0047}-supplemented diets, indicating that the presence of the dyes did not influence the larval food choice. In addition, fluorescence imaging of larvae fed for 30 min with probe-enriched liquid food indicated that both NRB^{MC009} and NRB^{ZLW0047} could be

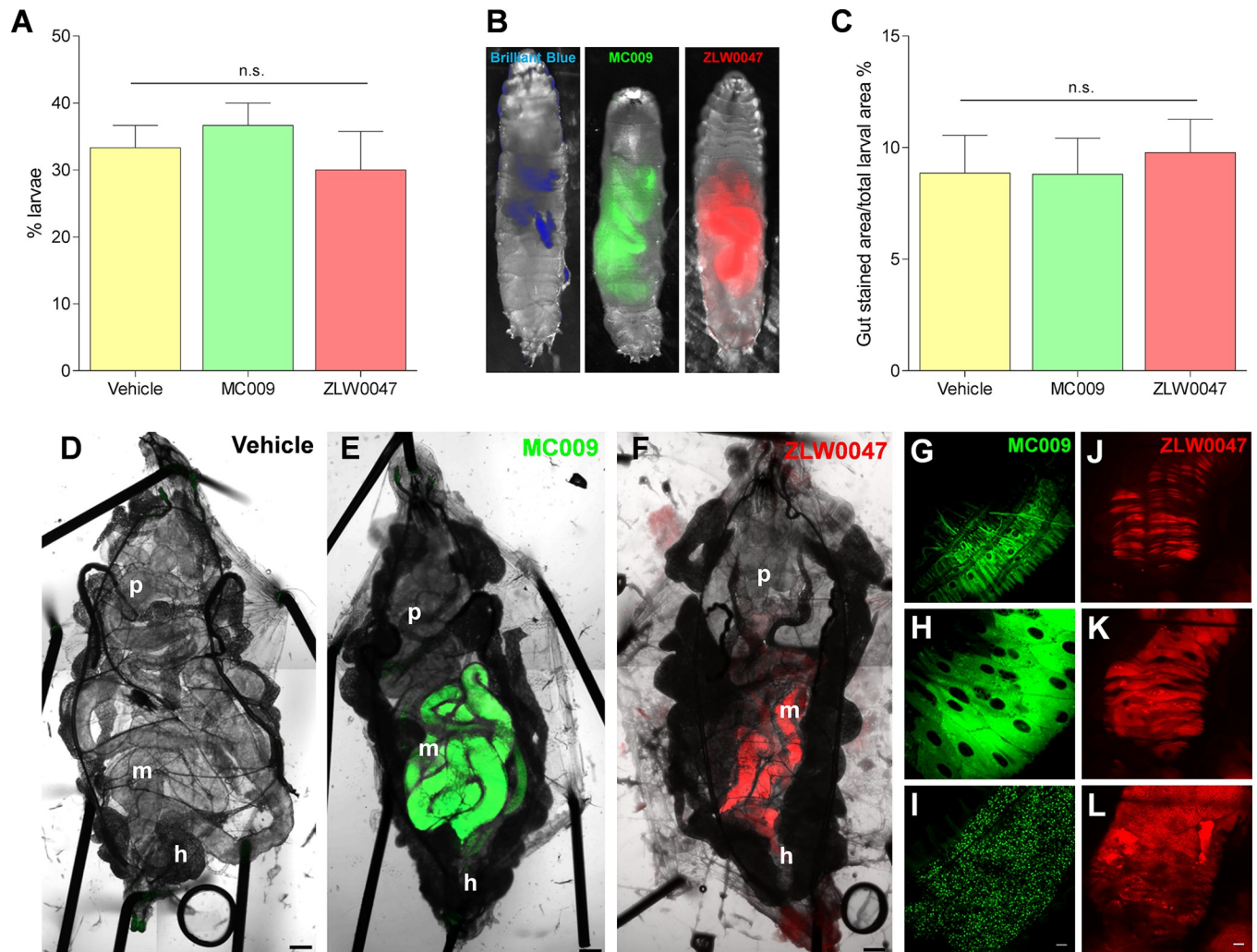


Fig 7. Use of NRB^{MC009} and NRB^{ZLW0047} as dyes for food intake tests. Quantification of larval dispersal after 5 minutes of three-choice preference assay of vehicle-added food, NRB^{MC009} 20 μ M -added food, or NRB^{ZLW0047} 20 μ M -added food (A). Data are expressed as percent of total larvae number and represent mean \pm SEM of five different experiments. Significance was calculated using One-way ANOVA test followed by Tukey's Multiple Comparison Test; n.s. $p > 0.05$. Representative images of larvae fed with liquid food supplemented with Brilliant blue R 0.08%, NRB^{MC009} 20 μ M, or NRB^{ZLW0047} 20 μ M, where gut was labeled by the three dyes (B) and quantification of gut stained area versus total larval area (C). Data are expressed as mean of percent \pm SEM of 30 larvae. Significance was calculated using One-way ANOVA test followed by Tukey's Multiple Comparison Test; n.s. $p > 0.05$. Confocal live imaging of whole dissected *Drosophila* third instar larva fed with vehicle-supplemented food (D), NRB^{MC009} 20 μ M-supplemented food (E), or NRB^{ZLW0047} 20 μ M-supplemented food (F); magnification 5x; scale bar 200 μ m. p: proventriculus, m: midgut, h: hindgut. Detailed images of mid gut external muscular cells (G, J), enterocytes (H, K) and intestinal food (I, L), labeled with the two NRB fluorescent derivatives; magnification 40x; scale bars 20 μ m.

<https://doi.org/10.1371/journal.pone.0211169.g007>

clearly detected in the gut (Fig 7B); a more in depth analysis revealed that gut fluorescence was regulated by the probes contained in the food, since no signal was observed in the gut wall, leading to the conclusion that the strength of the fluorescent signal could be taken as an index of the quantity of ingested food. Fig 7C reports the results of the food intake assay, expressed as a percentage of the gut stained area relative to the total body area—no significant difference was observed between larvae fed with NRB^{MC009}, NRB^{ZLW0047}, or brilliant blue dye, a commonly used dye for the evaluation of food intake in *Drosophila* [21].

The lack of gut labeling by NRB^{MC009} and NRB^{ZLW0047}, although a useful outcome for the food intake test, was somewhat unexpected, particularly considering the results obtained in the dissected larvae (see Figs 2 and 3) where the dyes were clearly localized to the intestinal

tract. To explain this inconsistency, we hypothesized that the time of exposure (30 min) of the larvae to the probe-supplemented food in the food intake assay was potentially too short to allow an internalization of the dyes to the gut epithelial cells. Therefore, we analyzed the gut wall of larvae grown for 5–7 days in food enriched with NRB^{MC009} or NRB^{ZLW0047}. Fig 7D–7F show the clear difference between vehicle-fed (Fig 7D) and NRB^{MC009}- and NRB^{ZLW0047}-fed larvae (Fig 7E and 7F, respectively). The bright fluorescent signal in the digestive tract (mainly midgut and hindgut) indicates that *Drosophila* larvae readily eat the probe-containing food. The digestive tract of NRB^{MC009}- and NRB^{ZLW0047}-fed larvae were clearly labeled by the dyes, a result that was accentuated by the absence of fluorescence in the rest of the body. The *Drosophila* intestinal tract is formed by a monolayer of epithelial cells, intestinal stem cells and enteroendocrine cells, surrounded by visceral muscles, nerves and tracheae. Ingested food from the proventriculus is pushed into the midgut, the main region of digestion and absorption, and then to the hindgut where the final absorption process takes place [13,14]. A deeper investigation on dissected *Drosophila* gut revealed that NRB^{MC009} and NRB^{ZLW0047} did not only label the food that was present and visible in the intestinal tract (Fig 7I and 7L), but they also bound to the gut external muscular cells (Fig 7G and 7J) and enterocytes (Fig 7H and 7K).

The bright fluorescence of NRB^{MC009} and NRB^{ZLW0047} make these probes eminently suitable for use in food intake tests and chronic feeding assays; as monitoring tools for abnormal gut morphology; and identifying defects in gut functionality during development or screening tests.

NRB^{MC009} and NRB^{ZLW0047} toxicity

In an attempt to validate the use of the NRB-derived fluorescent probes for use in chronic assays, we next verified their lack of toxicity in *Drosophila* by exposing the flies to NRB^{MC009} or NRB^{ZLW0047} over their entire life-cycle. The results indicate that male and female flies readily ingested NRB^{MC009}- and NRB^{ZLW0047}-supplemented food, mated and laid eggs normally, from which embryos hatched and larvae developed, grew, underwent pupation and eclosed in a similar fashion to non-treated flies. In addition, no difference in eclosion rate and lethality of adult flies was observed between probe-exposed and control flies (Fig 8A). Finally, we could

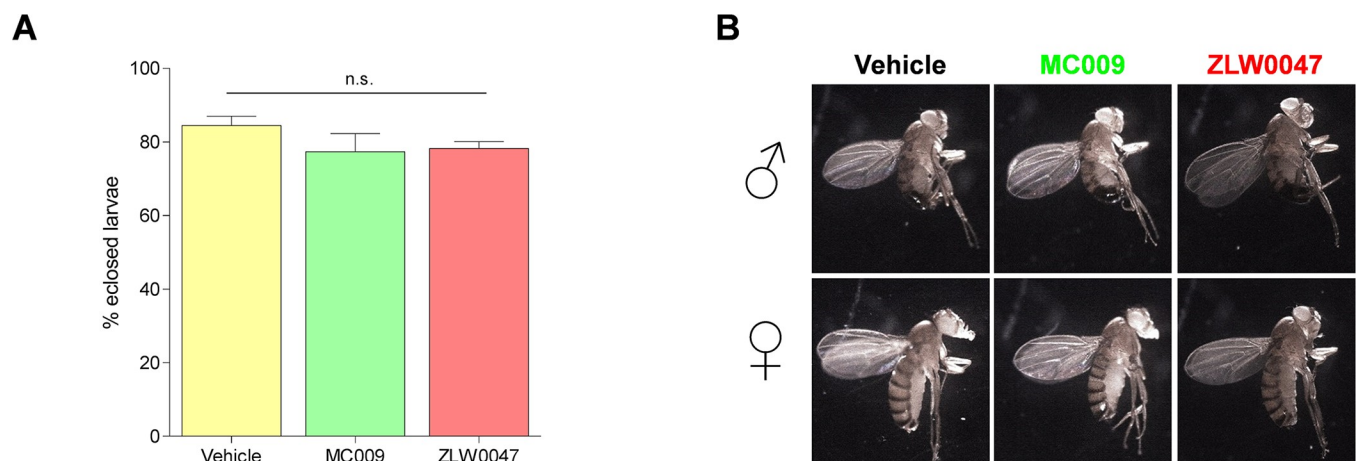


Fig 8. NRB^{MC009} and NRB^{ZLW0047} chronic toxicity. Evaluation of toxicity after exposition to standard food added with vehicle, NRB^{MC009} (20 μ M) or NRB^{ZLW0047} (20 μ M) over the *Drosophila* entire life-cycle. (A) Quantification of eclosion rate. Data are expressed as mean of percentages of emerged flies versus to the total number of pupae. Significance was calculated using One-way ANOVA test followed by Tukey's Multiple Comparison Test; n.s. $p > 0.05$. (B) Representative images of emerged male (σ) and female (ρ) w¹¹¹⁸ flies, where morphological alterations of body, eyes, wings, and legs were evaluated.

<https://doi.org/10.1371/journal.pone.0211169.g008>

not detect any apparent macroscopic morphological alteration in adult flies treated with either NRB^{MC009} or NRB^{ZLW0047} (Fig 8B).

The absence of toxicity and the high level of palatability supports NRB^{MC009} and NRB^{ZLW0047} as potential monitoring tools for long term feeding assays, as markers of intestinal epithelia, and their use in studying *Drosophila* digestive tract functionality e.g. monitoring the effect of compounds or diet on intestinal performance [35–37]. These attributes also make these probes potentially useful as mammalian gastrointestinal (GI) tract markers; for example, the GI tract is one of the most studied tissues in many pathological rodent models [38,39] and the availability of easy-to-use, high performance fluorescent probes to detect intracellular structure abnormalities could be of great benefit.

Overall, this study has investigated live cell imaging applications of NRB^{MC009} and NRB^{ZLW0047} in *Drosophila melanogaster*. The analysis of the fluorescent signals of these compounds reveal that both can label subcellular specific organelles (preferentially ER and mitochondria), in both wild type and pathological phenotypes. The absence of toxicity and the minimal effect on palatability also allows them to be used as potential monitoring tools in feeding assays, and as markers for intestinal epithelia that could be useful in *Drosophila* digestive tract studies. In summary, the characteristically bright signals of NRB^{MC009} and NRB^{ZLW0047}, in combination with their capacity to permeate tissues rapidly, makes them eminently suitable for confocal imaging applications. Our future studies will focus on investigating whether these compounds, with their enhanced attributes, may have potential to be used in invertebrate animal models.

Supporting information

S1 Fig. Confocal microscopes settings. Zeiss LSM800 Axio Observer Z1 inverted microscope and Nikon D-Eclipse C1 confocal microscope settings used (A). Summary table of laser intensity (%) and pinhole size (μm) used to capture NRB^{MC009} and NRB^{ZLW0047} in each tissue considered in the study (B).

(TIF)

S2 Fig. Larval tissues autofluorescence analysis. Confocal live cell images of unlabeled (A) leg imaginal disc, (B) muscles, (C) trachea, (D) oenocytes, (E) hindgut, (F) midgut, (G) fat body, (H) epidermis, (I) salivary gland, and (J) ring gland; magnification 40x; scale bars 20 μm . TL: transmitted light; green AF: autofluorescence using BODIPY-FL laser settings; red AF: autofluorescence using BODIPY-TMR laser settings. Quantification of NRB^{MC009} (K) and NRB^{ZLW0047} (L) fluorescence intensity without (dark bars) or with (light bars) autofluorescence subtraction in different larval tissues. Data are expressed as mean \pm SEM, $n \geq 5$; significance was calculated using unpaired t test; n.s. $p > 0.05$.

(TIF)

S3 Fig. NRB^{MC009} and NRB^{ZLW0047} internalization in larval muscles. Fluorescence intensity of NRB^{MC009} and NRB^{ZLW0047} internalization in dissected $w^{[1118]}$ larval muscles, extrapolated from a time-lapse image taken every 5 seconds for about 5 minutes. Data are expressed as mean \pm SEM, $n \geq 10$.

(TIF)

S4 Fig. NRB^{MC009} and NRB^{ZLW0047} do not label plasma membranes nor nuclei in larval tissues. Confocal live imaging of $w^{[1118]}$ larval (A) peripodal membrane cells of a leg imaginal disc, (B) salivary gland, (C) fat body, and (D) central nervous system labeled with NRB^{MC009} 500 nM (green) and CellMask Orange (cell membrane marker) 1 μM (red). Magnification 60x, scale bars 10 μm (A-C); magnification 40x, scale bar 100 μm (D). N: nucleus, G: ganglion, Nv:

nerves. Summary table of Pearson's correlation coefficients between NRB^{MC009} and CellMask in the evaluated tissues (E). Data are expressed as mean \pm SEM, $n \geq 10$. Confocal live imaging of UAS-mCD8-GFP/Tubulin-Gal4 (cell membrane marker) larval (F) peripodal membrane cells of a leg imaginal disc, (G) salivary gland, (H) fat body, and (I) central nervous system labeled with NRB^{ZLW0047} 1 μ M (red). Magnification 60x, scale bars 10 μ m (A-C); magnification 40x, scale bar 100 μ m (D). N: nucleus, G: ganglion, Nv: nerves. Summary table of Pearson's correlation coefficients between NRB^{ZLW0047} and mCD8-GFP signal in the evaluated tissues (L). Data are expressed as mean \pm SEM, $n \geq 10$.

(TIF)

S1 Video. Time-lapse of NRB^{MC009} internalization in dissected w^[1118] larval muscles, imaged every 5 seconds for about 5 minutes. Scale bar 20 μ m.

(AVI)

S2 Video. Time-lapse of NRB^{ZLW0047} internalization in dissected w^[1118] larval muscles, imaged every 5 seconds for about 5 minutes. Scale bar 20 μ m.

(AVI)

Author Contributions

Conceptualization: Alessia Forgiarini, Margaret Anne Brimble, Sergio Bova, David Rennison, Genny Orso.

Formal analysis: Alessia Forgiarini.

Funding acquisition: Brian Hopkins, Sergio Bova, David Rennison, Genny Orso.

Investigation: Alessia Forgiarini, Zifei Wang, Claudio D'Amore, Morgan Jay-Smith, Freda Fan Li, Andrea Pagetta, Sara Bersani, Barbara Napoli, David Rennison, Genny Orso.

Methodology: Alessia Forgiarini, Zifei Wang, Claudio D'Amore, Morgan Jay-Smith, Freda Fan Li, Andrea Pagetta, Sara Bersani, Barbara Napoli.

Project administration: Sergio Bova, David Rennison, Genny Orso.

Resources: Sergio Bova, David Rennison, Genny Orso.

Supervision: Margaret Anne Brimble, Sergio Bova, David Rennison, Genny Orso.

Validation: Genny Orso.

Visualization: Alessia Forgiarini.

Writing – original draft: Alessia Forgiarini, Sergio Bova, David Rennison, Genny Orso.

Writing – review & editing: Alessia Forgiarini, Zifei Wang, Freda Fan Li, Brian Hopkins, Margaret Anne Brimble, Sara De Martin, Sergio Bova, David Rennison, Genny Orso.

References

1. Roszkowski AP. The pharmacological properties of norbormide, a selective rat toxicant. *J Pharmacol Exp Ther.* 1965 Aug; 149(2):288–99. PMID: [4953462](https://pubmed.ncbi.nlm.nih.gov/4953462/)
2. Fusi F, Saponara S, Sgaragli G, Cargnelli G, Bova S. Ca²⁺ entry blocking and contractility promoting actions of norbormide in single rat caudal artery myocytes. *Br J Pharmacol.* 2002 Oct; 137(3):323–8. <https://doi.org/10.1038/sj.bjp.0704877> PMID: [12237251](https://pubmed.ncbi.nlm.nih.gov/12237251/)
3. Cavalli M, Omiciuolo L, Cargnelli G, Cima L, Hopkins B, Bova S. Distribution of the vasoconstrictor and vasorelaxant effects of norbormide along the vascular tree of the rat. *Life Sci.* 2004 Sep 17; 75(18):2157–65. <https://doi.org/10.1016/j.lfs.2004.04.022> PMID: [15325842](https://pubmed.ncbi.nlm.nih.gov/15325842/)

4. Bova S, Cima L, Golovina V, Luciani S, Cargnelli G. Norbormide: a Calcium Entry Blocker with Selective Vasoconstrictor Activity in Rat Peripheral Arteries. *Cardiovasc Drug Rev*. 2001 Sep 1; 19(3):226–33. PMID: [11607040](#)
5. D'Amore C, Orso G, Fusi F, Pagano MA, Miotto G, Forgiarini A, et al. An NBD Derivative of the Selective Rat Toxicant Norbormide as a New Probe for Living Cell Imaging. *Front Pharmacol*. 2016 Sep; 7.
6. D'Amore C, Orso G, Forgiarini A, Ceolotto G, Rennison D, Ribauda G, et al. Synthesis and Biological Characterization of a New Norbormide Derived Bodipy FL-Conjugated Fluorescent Probe for Cell Imaging. *Front Pharmacol*. 2018 Sep 25; 9:1055. <https://doi.org/10.3389/fphar.2018.01055> PMID: [30319407](#)
7. Aldaz S, Escudero LM, Freeman M. Live imaging of *Drosophila* imaginal disc development. *Proc Natl Acad Sci U S A*. 2010 Aug; 107(32):14217–22. <https://doi.org/10.1073/pnas.1008623107> PMID: [20660765](#)
8. Tan FHP, Azzam G. *Drosophila melanogaster*: Deciphering Alzheimer's Disease. *Malays J Med Sci MJMS*. 2017 Mar; 24(2):6–20. <https://doi.org/10.21315/mjms2017.24.2.2> PMID: [28894399](#)
9. Musselman LP, Kühnlein RP. *Drosophila* as a model to study obesity and metabolic disease. *J Exp Biol*. 2018 Mar 7; 221(Pt Suppl 1):jeb163881.
10. Chatterjee S. Artefacts in histopathology. *J Oral Maxillofac Pathol JOMFP*. 2014 Sep; 18(Suppl 1): S111–6. <https://doi.org/10.4103/0973-029X.141346> PMID: [25364159](#)
11. Mushtaq Z, Choudhury SD, Gangwar SK, Orso G, Kumar V. Human Senataxin Modulates Structural Plasticity of the Neuromuscular Junction in *Drosophila* through a Neuronally Conserved TGF β Signaling Pathway. *Neurodegener Dis*. 2016; 16(5–6):324–36. <https://doi.org/10.1159/000445435> PMID: [27197982](#)
12. Orso G, Martinuzzi A, Rossetto MG, Sartori E, Feany M, Daga A. Disease-related phenotypes in a *Drosophila* model of hereditary spastic paraplegia are ameliorated by treatment with vinblastine. *J Clin Invest*. 2005 Nov 1; 115(11):3026–34. <https://doi.org/10.1172/JCI24694> PMID: [16276413](#)
13. Kuraishi T, Kenmoku H, Kurata S. From mouth to anus: Functional and structural relevance of enteric neurons in the *Drosophila melanogaster* gut. *Insect Biochem Mol Biol*. 2015 Dec; 67:21–6. <https://doi.org/10.1016/j.ibmb.2015.07.003> PMID: [26232723](#)
14. Lemaitre B, Miguel-Aliaga I. The Digestive Tract of *Drosophila melanogaster*. *Annu Rev Genet*. 2013; 47(1):377–404.
15. Limmer S, Weiler A, Volkenhoff A, Babatz F, Klämbt C. The *Drosophila* blood-brain barrier: development and function of a glial endothelium. *Front Neurosci*. 2014 Nov; 8.
16. Meltola NJ, Wahlroos R, Soini AE. Hydrophilic Labeling Reagents of Dipyrromethene-BF₂ Dyes for Two-Photon Excited Fluorometry: Syntheses and Photophysical Characterization. *J Fluoresc*. 2004 Sep 1; 14(5):635–47. PMID: [15617270](#)
17. Rennison D, Laita O, Conole D, Jay-Smith M, Knauf J, Bova S, et al. Prodrugs of N-dicarboximide derivatives of the rat selective toxicant norbormide. *Bioorg Med Chem*. 2013 Sep 15; 21(18):5886–99. <https://doi.org/10.1016/j.bmc.2013.06.071> PMID: [23920483](#)
18. Orso G, Penden D, Liu S, Tosetto J, Moss TJ, Faust JE, et al. Homotypic fusion of ER membranes requires the dynamin-like GTPase atlastin. *Nature*. 2009 Aug 20; 460(7258):978–83. <https://doi.org/10.1038/nature08280> PMID: [19633650](#)
19. Kassan A, Herms A, Fernández-Vidal A, Bosch M, Schieber NL, Reddy BJN, et al. Acyl-CoA synthetase 3 promotes lipid droplet biogenesis in ER microdomains. *J Cell Biol*. 2013 Dec 23; 203(6):985–1001. <https://doi.org/10.1083/jcb.201305142> PMID: [24368806](#)
20. Kim D, Alvarez M, Lechuga LM, Louis M. Species-specific modulation of food-search behavior by respiration and chemosensation in *Drosophila* larvae. *eLife*. 2017 Sep 5; 6:e27057. <https://doi.org/10.7554/eLife.27057> PMID: [28871963](#)
21. Kaun KR, Riedl CAL, Chakabarty-Chatterjee M, Belay AT, Douglas SJ, Gibbs AG, et al. Natural variation in food acquisition mediated via a *Drosophila* cGMP-dependent protein kinase. *J Exp Biol*. 2007 Oct 15; 210(20):3547–58.
22. Schindelin J, Arganda-Carreras I, Frise E, Kaynig V, Longair M, Pietzsch T, et al. Fiji: an open-source platform for biological-image analysis. *Nat Methods*. 2012 Jul; 9(7):676–82. <https://doi.org/10.1038/nmeth.2019> PMID: [22743772](#)
23. Vanni S. Intracellular Lipid Droplets: From Structure to Function. *Lipid Insights* [Internet]. 2017 Dec 13 [cited 2018 Nov 15]; 10. Available from: <https://www.ncbi.nlm.nih.gov/pmc/articles/PMC5731618/>
24. Papadopoulou C, Orso G, Mancuso G, Herholz M, Gumeni S, Tadepalle N, et al. Spastin binds to lipid droplets and affects lipid metabolism. *PLoS Genet*. 2015 Apr; 11(4):e1005149. <https://doi.org/10.1371/journal.pgen.1005149> PMID: [25875445](#)

25. Wang Z-H, Clark C, Geisbrecht ER. Analysis of mitochondrial structure and function in the *Drosophila* larval musculature. *Mitochondrion*. 2016 Jan; 26:33–42. <https://doi.org/10.1016/j.mito.2015.11.005> PMID: 26611999
26. Kreipke RE, Kwon Y V., Shcherbata HR, Ruohola-Baker H. *Drosophila melanogaster* as a Model of Muscle Degeneration Disorders. *Curr Top Dev Biol*. 2017; 121:83–109. <https://doi.org/10.1016/bs.ctdb.2016.07.003> PMID: 28057309
27. Beckett K, Baylies MK. The Development of The *Drosophila* Larval Body Wall Muscles. In: *International Review of Neurobiology*. Academic Press; 2006. p. 55–70. (The Fly Neuromuscular Junction: Structure and Function Second Edition; vol. 75).
28. Hirth F. *Drosophila melanogaster* in the Study of Human Neurodegeneration. *CNS Neurol Disord Drug Targets*. 2010 Aug; 9(4):504–23. <https://doi.org/10.2174/187152710791556104> PMID: 20522007
29. McGurk L, Berson A, Bonini NM. *Drosophila* as an In Vivo Model for Human Neurodegenerative Disease. *Genetics*. 2015 Oct; 201(2):377–402. <https://doi.org/10.1534/genetics.115.179457> PMID: 26447127
30. Rossetto MG, Zanarella E, Orso G, Scorzeto M, Megighian A, Kumar V, et al. Defhc1.1, a homologue of the juvenile myoclonic gene EFHC1, modulates architecture and basal activity of the neuromuscular junction in *Drosophila*. *Hum Mol Genet*. 2011 Nov 1; 20(21):4248–57. <https://doi.org/10.1093/hmg/ddr352> PMID: 21835885
31. Yamaguchi M, Takashima H. *Drosophila* Charcot-Marie-Tooth Disease Models. In: Yamaguchi M, editor. *Drosophila Models for Human Diseases* [Internet]. Singapore: Springer Singapore; 2018 [cited 2018 Nov 5]. p. 97–117. (Advances in Experimental Medicine and Biology). Available from: https://doi.org/10.1007/978-981-13-0529-0_7
32. Ozdowski EF, Baxter SL, Sherwood NT. Chapter 73—*Drosophila* Models of Hereditary Spastic Paraplegia. In: LeDoux MS, editor. *Movement Disorders (Second Edition)* [Internet]. Boston: Academic Press; 2015 [cited 2018 Nov 5]. p. 1103–22. Available from: <http://www.sciencedirect.com/science/article/pii/B9780124051959000731>
33. Nakhro K, Park J-M, Choi B-O, Chung KW. Missense mutations of mitofusin 2 in axonal Charcot-Marie-Tooth neuropathy: polymorphic or incomplete penetration? *Anim Cells Syst*. 2013 Aug; 17(4):228–36.
34. Debattisti V, Pendin D, Ziviani E, Daga A, Scorrano L. Reduction of endoplasmic reticulum stress attenuates the defects caused by *Drosophila* mitofusin depletion. *J Cell Biol*. 2014 Feb; 204(3):303–12. <https://doi.org/10.1083/jcb.201306121> PMID: 24469638
35. Apidianakis Y, Rahme LG. *Drosophila melanogaster* as a model for human intestinal infection and pathology. *Dis Model Mech*. 2011 Jan; 4(1):21–30. <https://doi.org/10.1242/dmm.003970> PMID: 21183483
36. Storelli G, Strigini M, Grenier T, Bozonnet L, Schwarzer M, Daniel C, et al. *Drosophila* Perpetuates Nutritional Mutualism by Promoting the Fitness of Its Intestinal Symbiont *Lactobacillus plantarum*. *Cell Metab*. 2018 Feb 6; 27(2):362–377.e8. <https://doi.org/10.1016/j.cmet.2017.11.011> PMID: 29290388
37. Gasque G, Conway S, Huang J, Rao Y, Vosshall LB. Small molecule drug screening in *Drosophila* identifies the 5HT2A receptor as a feeding modulation target. *Sci Rep*. 2013; 3:srep02120. <https://doi.org/10.1038/srep02120> PMID: 23817146
38. Caputi V, Marsilio I, Filpa V, Cerantola S, Orso G, Bistoletti M, et al. Antibiotic-induced dysbiosis of the microbiota impairs gut neuromuscular function in juvenile mice. *Br J Pharmacol*. 2017 Oct 1; 174(20):3623–39. <https://doi.org/10.1111/bph.13965> PMID: 28755521
39. Antonioli L, Pellegrini C, Fornai M, Tirota E, Gentile D, Benvenuti L, et al. Colonic motor dysfunctions in a mouse model of high-fat diet-induced obesity: an involvement of A2B adenosine receptors. *Purinergic Signal*. 2017 Dec 1; 13(4):497–510. <https://doi.org/10.1007/s11302-017-9577-0> PMID: 28808842